ISSN 0735-2727, Radioelectronics and Communications Systems, 2023, Vol. 66, No. 5, pp. 251–262. © Allerton Press, Inc., 2023.
Ukrainian Text © The Author(s), 2023, published in Izvestiya Vysshikh Uchebnykh Zavedenii, Radioelektronika, 2023, Vol. 66, No. 5, pp. 293–304.

Patch Antennas Based on Micro QR Codes

V. Slyusar[a, *] (ORCID: 0000-0002-2912-3149),
I. Sliusar[b, **] (ORCID: 0000-0003-1197-5666),
and S. Sheleg[c, *] (ORCID: 0000-0002-1378-2617)**

[a]*Central Research Institute of Armaments and Military Equipment of Armed Forces of Ukraine, Kyiv, Ukraine*
[b]*Poltava State Agrarian University, Poltava, Ukraine*
[c]*ENIT, Inc., Scottsdale, AZ, USA*
**e-mail: swadim@ukr.net*
***e-mail: islyusar2007@ukr.net*
****e-mail: ssheleg@yahoo.com*

Received October 5, 2022; revised April 4, 2023; accepted May 1, 2023

Abstract—The article proposes a new type of broadband patch antennas based on micro QR codes with integrated metamaterial cell as a marker. In this research, several design options were considered that used the variation of the metamaterial cell parameters. For their analysis, the numerical modeling methods of the Ansys EM Suite program were used due to the complexity of describing the interaction of antennas of non-Euclidean geometry with radio waves. Evaluation and comparison of proposed antennas was conducted by the following characteristics: amplitude-frequency response and voltage standing wave ratio. To expand the frequency band of the synthesized antenna has been implemented the split square marker is an element of micro QR. This approach enables the expansion of the relative bandwidth of the corresponding printed antenna to the value of 1.7267 under the condition of the continuous transmission band having a width of 167.935 GHz within the range from 13.29 to 181.225 GHz. In this case, cutouts of the split square marker are located along the line coaxial with the power supply line, and the cutout for the outer "ring" is located below. To synthesize micro QR code, the word "antenna" was used.

Keywords: amplitude-frequency response, Ansys HFSS, metamaterial, micro QR, patch antenna, power supply, return loss, voltage standing wave ratio, VSWR

DOI: 10.3103/S073527272307004X

1. INTRODUCTION

The development of communication systems of the 6th generation (6G) is based on the application of new approaches and technical solutions. Further evolution of the antenna systems with regard to 6G trend will imply the following courses [1]–[3]: an increase of the number of antenna elements within the antenna array in Massive MIMO and Super-Massive MIMO systems (32×32 and so on); the transfer to the working frequencies of terahertz range, integration of several broadband frequency ranges within one antenna design, including the terahertz range as well; photonic technologies and neural networks for the beamforming and signal processing; combination of the functionality of the radar and communication system for observing and steering of the unmanned swarm systems, such as unmanned air vehicles (UAVs), unmanned ground vehicles (UGVs), unmanned surface vehicles (USVs).

One of the approaches to creating 6G systems is the use of intelligent reflective surfaces (IRS) [4]. IRS can be used as an intelligent repeater for multiple transmitters in complex cellular communications and radar systems [5]. At the same time, placing the IRS on the walls of buildings and public access facilities, as well as on interior furniture and equipment inside the premises, will expand the functionality of IRS by creating various advertising images using reflective elements.

Particularly, IRS is proposed to be used as a platform to collect multiple QR codes, providing access to various websites containing advertising content. In this case, the forming of images of QR codes can be performed based on the principle of hierarchy when one or several large sized QR codes, formed by the mass of smaller QR codes, are visually reproduced at a sufficient distance. In turn, these smaller ones can be formed based on QR codes which will be perceived while being only in close proximity to the IRS surface.

In cases when the monotypic QR codes are used at different levels of the hierarchies, factually, it refers to the fractal approach which can be formalized as a matrix using the Kronecker product of matrices. For example, if the primary QR code is represented as a matrix of pixels A, then the fractal system of three iterations of such codes can be represented as follows:

$$\mathbf{H} = \mathbf{A} \otimes \mathbf{A} \otimes \mathbf{A}, \tag{1}$$

where $\otimes$ is a symbol of the operation of Kronecker product.

In this case, each pixel of the large image is replaced by the matrix of the same QR code within the limits of a single pixel. The same procedure takes place again during the next iteration.

If a separate code is used for each iteration, then the expression (1) should be restated as follows:

$$\mathbf{H} = \mathbf{A} \otimes \mathbf{B} \otimes \mathbf{C}. \tag{2}$$

Matrices **A**, **B**, and **C** can represent not only different coded pieces of information within the same QR code connected, for example, semantically, but different types of codes as well: QR, micro QR, and so on.

When moving to the lower level of micro QR codes, the penetrating face product of matrices [6], [7] can be used to describe pixel topologies. According to the definition [6], the penetrating face product of a (p×g)-matrix **A** and an n-dimensional tensor **B** expanded into a block matrix containing (p×g) blocks (**B** = [$\mathbf{B}_n$], $n > 1$) is the following matrix type:

$$\mathbf{A}[\circ]\mathbf{B} = [\mathbf{A} \circ \mathbf{B}_n], \tag{3}$$

where $\mathbf{A} \circ \mathbf{B}_n$ is the Hadamard product.

If matrix **A** represents pixels of the micro QR codes at the low level, and the block matrix **B** represents the pixels clusters of the micro QR or QR codes at the high level, then the topology of results is described as follows:

$$\mathbf{A}[\circ]\mathbf{B} = \mathbf{A}[\circ]\begin{bmatrix} B_{11} & B_{12} & \cdots & B_{1G} \\ B_{21} & B_{22} & \cdots & B_{2G} \\ \vdots & \vdots & \ddots & \vdots \\ B_{P1} & B_{P2} & \cdots & B_{PG} \end{bmatrix} = \begin{bmatrix} \mathbf{A} \circ B_{11} & \mathbf{A} \circ B_{12} & \cdots & \mathbf{A} \circ B_{1G} \\ \mathbf{A} \circ B_{21} & \mathbf{A} \circ B_{22} & \cdots & \mathbf{A} \circ B_{2G} \\ \vdots & \vdots & \ddots & \vdots \\ \mathbf{A} \circ B_{P1} & \mathbf{A} \circ B_{P2} & \cdots & \mathbf{A} \circ B_{PG} \end{bmatrix}. \tag{4}$$

As an example,

$$\mathbf{A} = \begin{bmatrix} a_{11} & a_{12} \\ a_{21} & a_{22} \\ a_{31} & a_{32} \end{bmatrix},$$

$$\mathbf{B} = \begin{bmatrix} b_{111} & b_{121} & b_{112} & b_{122} & b_{113} & b_{123} \\ b_{211} & b_{221} & b_{212} & b_{222} & b_{213} & b_{223} \\ b_{311} & b_{321} & b_{312} & b_{322} & b_{313} & b_{323} \end{bmatrix},$$

$$\mathbf{A}[\circ]\mathbf{B} = \begin{bmatrix} a_{11} \cdot b_{111} & a_{12} \cdot b_{121} & a_{11} \cdot b_{112} & a_{12} \cdot b_{122} & a_{11} \cdot b_{113} & a_{12} \cdot b_{123} \\ a_{21} \cdot b_{211} & a_{22} \cdot b_{221} & a_{21} \cdot b_{212} & a_{22} \cdot b_{222} & a_{21} \cdot b_{213} & a_{22} \cdot b_{223} \\ a_{31} \cdot b_{311} & a_{32} \cdot b_{321} & a_{31} \cdot b_{312} & a_{32} \cdot b_{322} & a_{31} \cdot b_{313} & a_{32} \cdot b_{323} \end{bmatrix}.$$

If it is necessary to use different QR codes within the same fractal iteration, then it is necessary to apply the block Kronecker product of matrices [8] to formalize the topology of such IRS. At that, the primary

matrix of QR code is divided into M modules, either of which is multiplied then by its corresponding matrix of the next iteration using the direct Kronecker product:

$$H = \begin{bmatrix} A_1 & A_2 & \dots & A_M \end{bmatrix} [\otimes] \begin{bmatrix} B_1 & B_2 & \dots & B_M \end{bmatrix} [\otimes] \begin{bmatrix} C_1 & C_2 & \dots & C_M \end{bmatrix}, \quad (5)$$

where [⊗] is a symbol of the operation of the block Kronecker product.

The combination of both indicated options with the monotypic pixel filling within one iteration as well as diversified one at the other levels of hierarchy is possible, for example:

$$H = \left(\begin{bmatrix} A_1 & A_2 & \dots & A_M \end{bmatrix} \otimes B \right) [\otimes] \begin{bmatrix} C_1 & C_2 & \dots & C_M \end{bmatrix}, \quad (6)$$

$$H = \begin{bmatrix} A_1 & A_2 & \dots & A_M \end{bmatrix} [\otimes] \begin{bmatrix} A_1 & A_2 & \dots & A_M \end{bmatrix} [\otimes] \begin{bmatrix} C_1 & C_2 & \dots & C_M \end{bmatrix}, \quad (7)$$

and so on.

Given that IRS can be both passive and active, the proposal is to coat the IRS surfaces with the QR codes made of conductive materials and thus create printed antennas in the form of QR code.

It should be noted that the idea of application of QR codes for the topology of antennas is not a new one. For example, publication [9] can be noted among the first ones in this regard. The further development of this direction about the printed antennas was represented in works [10]–[14]. Specifically, in paper [10] the option of the antenna with the power supply leads switched to one of the internal pixels within the body of QR code had been considered. Such a decision has limited possibilities with regard to the antenna arrangement, which has impeded the possibility of obtaining a return loss level less than –8 dB, moreover, within a very narrow frequency range.

The same approach with intrapixel switch of the power supply leads has been studied in [11]. In this case, the authors of the paper [11] were able to obtain rather low values of the return loss (–21.48 dB) within the narrow frequency range at 2.4 GHz utilizing the smart choice of the code phrase as well as optimization of the positioning of the connecting modules in the topology of QR code considering 7-percent mistake correction during its decoding.

Paper [12] has made a further step for the development of the concept of optimization of QR-antenna parameters with the intrapixel supply based on the input of the intentional distortions in the topology of QR code. According to it, the conventional antenna of RFID tag was integrated with the topology of QR code, and as a result, the return loss was obtained at the level of –15.4 dB at the resonant frequency of 2.45 GHz, along with the widening of the working frequency transmission band from 2.3 to 3.08 GHz.

Meanwhile, it should be noted that the concept of the input of intentional distortions into the structure of QR code for the optimization of antenna parameters, proposed in [11], [12], has limited possibilities about the widening of their bandwidth. The application of the supply lines, external to the topology of QR antennas, provides more degrees of freedom concerning obtaining broadbandness.

For example, the option of such supply leads deployment in the form of a strip line outside the outline of QR code, performing the function of the external resonator, which enables us to widen the operating band of the antenna, has been proposed in paper [13]. The switch of the strip supply line to several pixels of the external outline of QR code described in the paper [14] is worth noticing in the context of the approach reviewed in the present article.

As it was previously mentioned, the micro QR codes can be used along with QR codes for the design synthesis of printed antennas within IRS. The potential options for the topology of such antennas are proposed and studied in the paper [15]. Let us consider further development of the present antenna solutions in the frame of the hypothesis, formulated in the paper [15], concerning the appropriate use of metamaterial unit structure elements of the reference segment of micro QR code.

The rest of the paper is organized in a structured manner, with several sections to help readers navigate the content. Section 2 describes the approach taken by the authors to develop and test their printed antenna design. This includes a detailed description of the Ansys EM Suite software used to create the design, as well as specific parameters and variables used in the model. Section 3 presents the findings of the study, including the VSWR and return loss values of the synthesized antenna, as well as its radiation pattern at a frequency of 25 GHz. The authors compare their results to previous studies and discuss the implications of their findings in Section 4. Finally, the paper concludes with a discussion of the main contributions of the study, its limitations, and areas for future research.

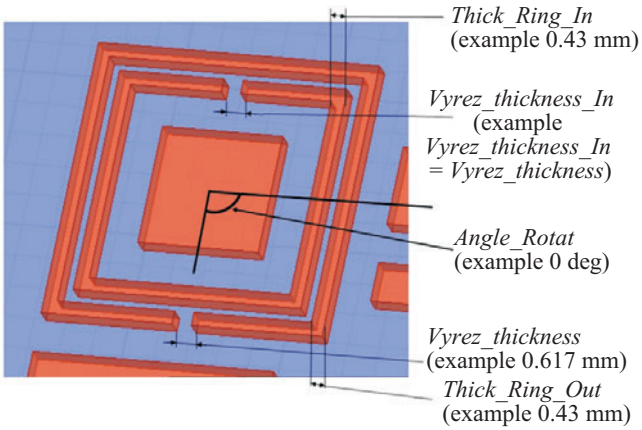

Fig. 1. SRR-frame around reference square pattern of micro QR code.

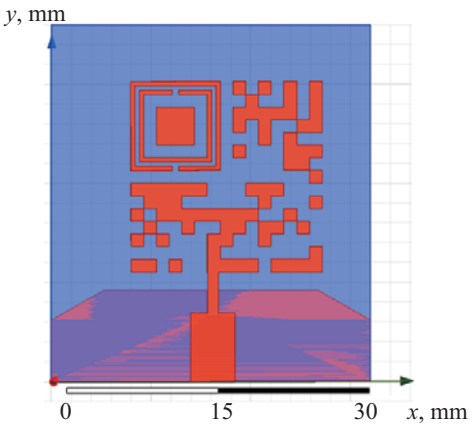

Fig. 2. Design of patch antenna.

Table 1. Design parameters

Parameter	Variable	Value
Width of inner ring	Thick_Ring_In	0.43 mm
Width of outer ring	Thick_Ring_Out	0.43 mm
Width of cutout in inner ring	Vyrez_thickness_In	0.617 mm
Width of cutout in outer ring	Vyrez_thickness	0.617 mm
Rotation angle	Angle_rotat	0 deg

2. PROPOSED DESIGN OF PATCH ANTENNA BASED ON MICRO QR CODE

For the research execution, the authors have developed the base model of the patch antenna based on micro QR code containing the word "antenna" in Ansys EM Suite software package [16]. The formation of the topology corresponding to the specific code had been performed similarly to [15] using services [17] and [18]. The choice of the word "antenna" enables us to preserve the continuation of the results of the paper [15] as well as to perform the comparison of the features of previously synthesized antennas with their new topologies.

The novelty of the proposed approach lies in the fact that within the indicated base model, the unit of metamaterial in the form of a pair of dissected square patterns (SRR-resonator [19]–[21]) has been used, outlining the reference square pattern in the left upper corner of the microcode matrix (Fig. 1). At that, the width of the cutout can be changed within SRR (variables *Vyrez_thickness* (cutout) – outer ring, *Vyrez_thickness_In* (cutout) – inner ring). All variables are set in mm. As a default, it is established that *Vyrez_thickness_In* = *Vyrez_thickness*. The orientation of the cutout in SRR is set for the outer ring of the variable *Angle_rotat* (0, 90, 180, 270 deg), and for the inner ring it is replaced by the variable *Angle_rotat_In* within the default set of the similar values: 0, 90, 180, 270 deg.

In this case, 0° corresponds to the location of the cutout for the outer and inner rings below the frame, on the axis parallel to the power supply line.

The width of SRR frames (in mm) within the model is set up by variables: *Thick_Ring_In*—for the inner ring, and *Thick_Ring_Out*—for the outer one. In this case, the main requirement is to meet the following condition:

$$\left(Thick\_Ring\_In + Thick\_Ring\_Out\right) \le 1.28 \text{ mm}.$$

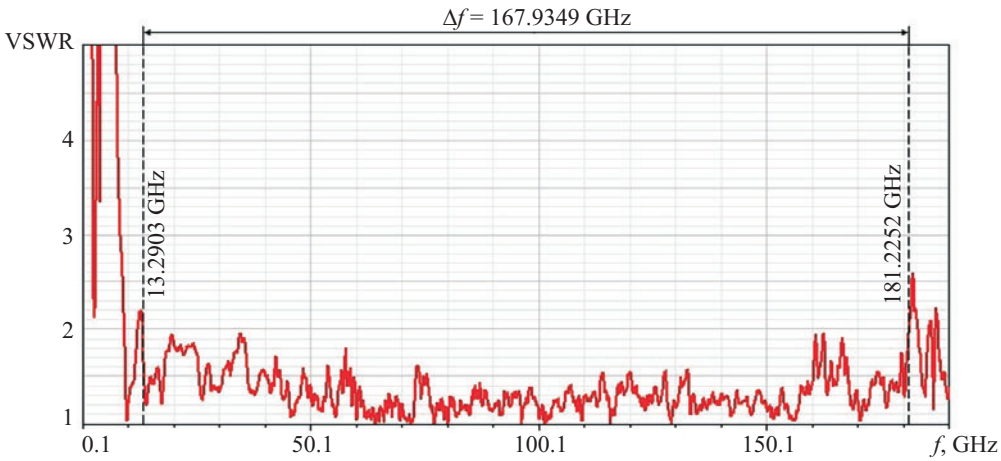

Fig. 3. VSWR of antenna in Fig. 2.

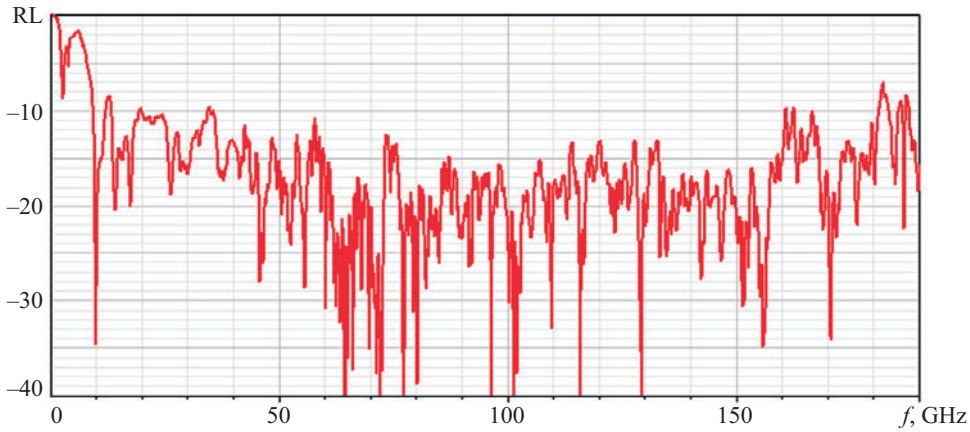

Fig. 4. RL of antenna in Fig. 2.

It is connected with the provision of the possibility for the decoding of micro QR codes in typical smartphone applications. Instead of the standard frame width of the reference square pattern of 1 mm, the width of 1.28 mm has been set up, which is connected with the scaling of micro QR code for binding it with the result of the authors' other publications [15].

The general view of the proposed printed antenna is presented in Fig. 2. The cutout in the outer ring is located below. Both cutouts are positioned along the line coaxial to the power supply line. The values of the key parameters of the design are presented in Table 1.

Regarding the parameters of the power supply line and configuration of the screen, all the topology options reviewed here, have been set up as identical to the antennas [15].

The modification of the code matrix (Fig. 2) was tested about the possibility of decoding by the scanner of iPhone 11 Pro, following the condition of the color change for all the pixel elements of the code to black. Then, despite the cutouts in the reference frame, the word "antenna" had been scanned even in case of minor disturbances in the harmonization of the flat surface and smartphone orientation towards the surface of the display engaged into the projection of the antenna topology in Ansys EM Suite program.

3. RESEARCH RESULTS OF BASIC ANTENNA MODEL

The results of the calculation of voltage standing wave ratio (VSWR) and the return loss (RL) of the synthesized antenna, which are the conventional parameters for the analysis of characteristics of antennas [22], [23], are presented in Figs. 3 and 4, respectively.

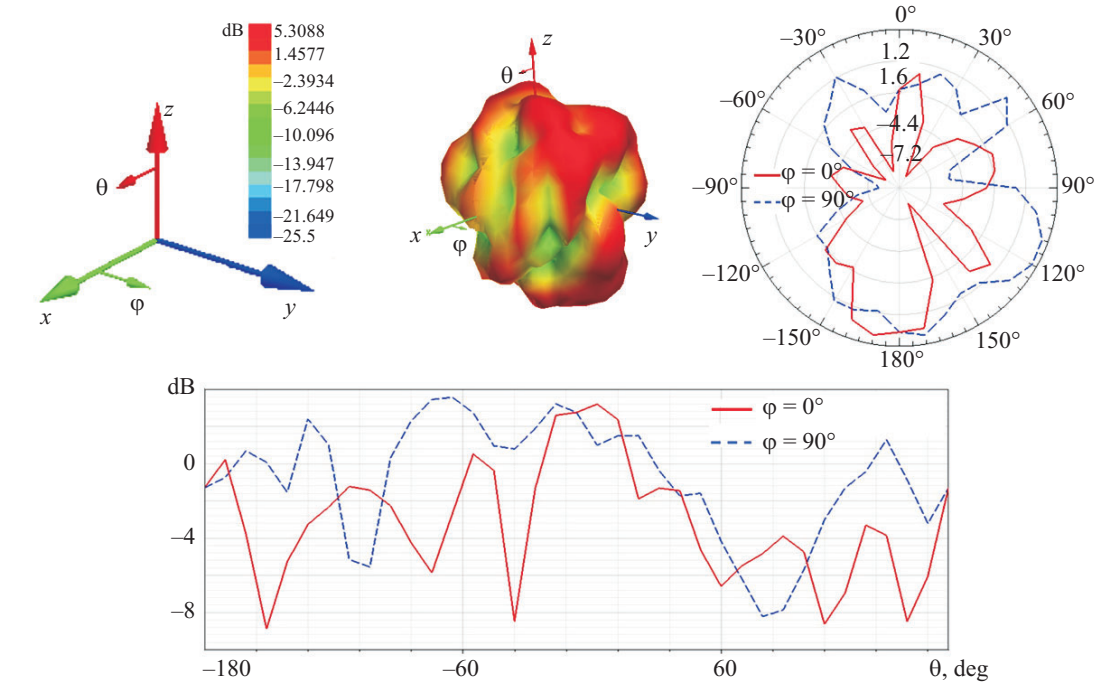

Fig. 5. Radiation pattern of antenna under consideration at 25 GHz.

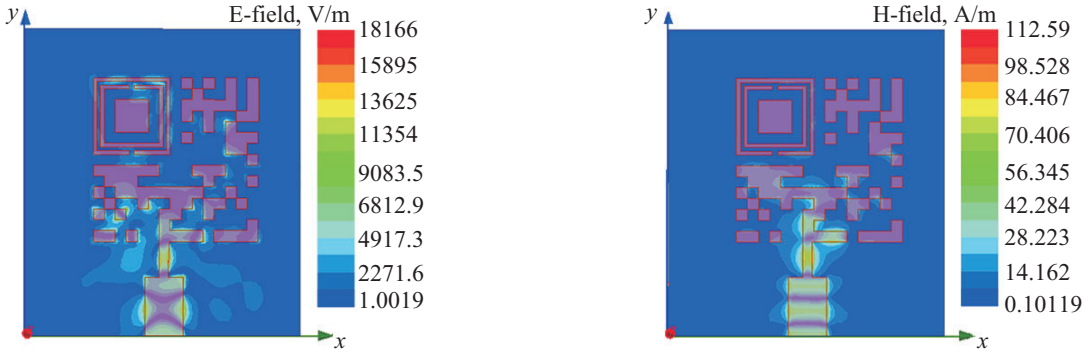

Fig. 6. E- and H-fields distributions on surface of substrate of antenna under consideration at 25 GHz.

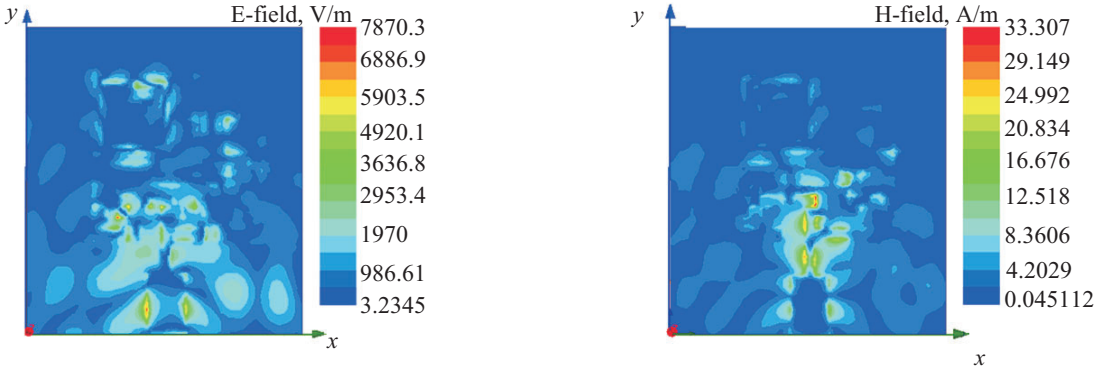

Fig. 7. E- and H-fields distributions on upper surface of antenna under consideration at 25 GHz.

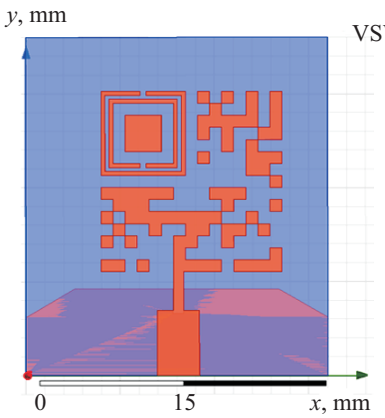

Fig. 8. Alternative option of printed antenna.

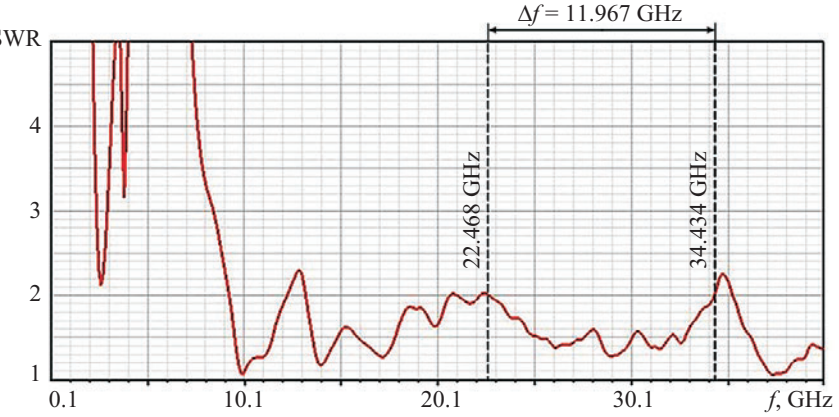

Fig. 9. VSWR of antenna in Fig. 8.

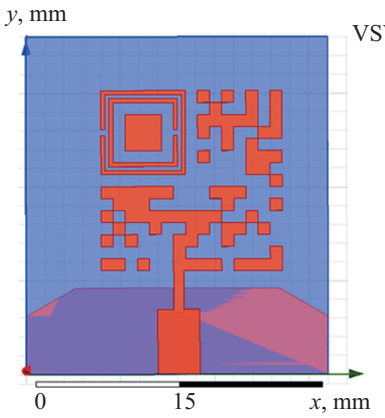

Fig. 10. Printed antenna with horizontal location of cutouts in reference element.

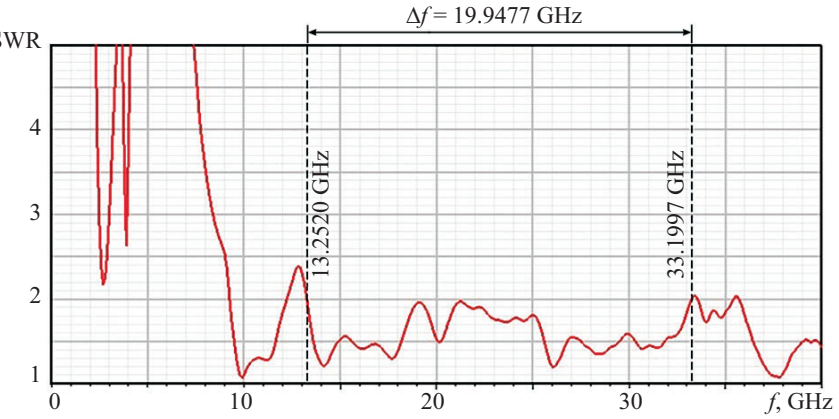

Fig. 11. VSWR of antenna in Fig. 10.

The application of the metaunit as the reference element made it possible to eliminate the peaks within the range of 19–20 GHz, which were present in printed antenna in the form of the primary micro QR code [15]. It provided the continuous transmission band with a width of 167.935 GHz within the range from 13.29 to 181.225 GHz. In this case, the relative bandwidth [24]:

$$\delta F = \frac{2|f_1 - f_2|}{f_1 + f_2} = 1.7267, \tag{8}$$

where f_1 and f_2 are the values of the frequencies at which VSWR = 2.

Therefore, the obtained modeling data confirmed the hypothesis about the efficiency of the application of SRR metaunit in the form of a passive element within the printed antenna. The frequency range from 13.29 to 181.225 GHz covers all possible millimeter ranges of 5G and 6G waves, such as FR2 spanning from 24.25 to 52.6 GHz (NR Rel-15), [25] and FR2-2 from 52.6 to 71 GHz (NR Rel-17) [26].

The radiation pattern of the antenna under consideration for a frequency of 25 GHz is shown in Fig. 5 in 3D and 2D formats. It is important to emphasize that the radiation pattern will vary depending on the bandwidth, and this may affect the use of such elements in IRS.

As an additional illustration of the properties of the antenna, Figs. 6 and 7 show E- and H-fields distributions on the surface of the substrate and the upper surface of the antenna.

As follows from Fig. 7, the main contribution to the antenna radiation comes from micro QR code elements localized in the feeder zone. In this case, SRR acts as a passive element that corrects the main radiation field.

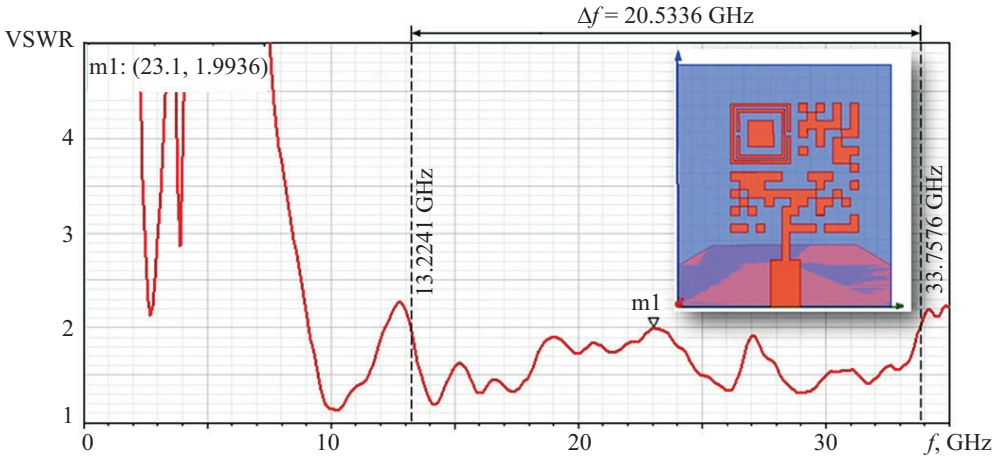

Fig. 12. Alternative option of printed antenna with horizontal location of cutouts in reference element and its VSWR.

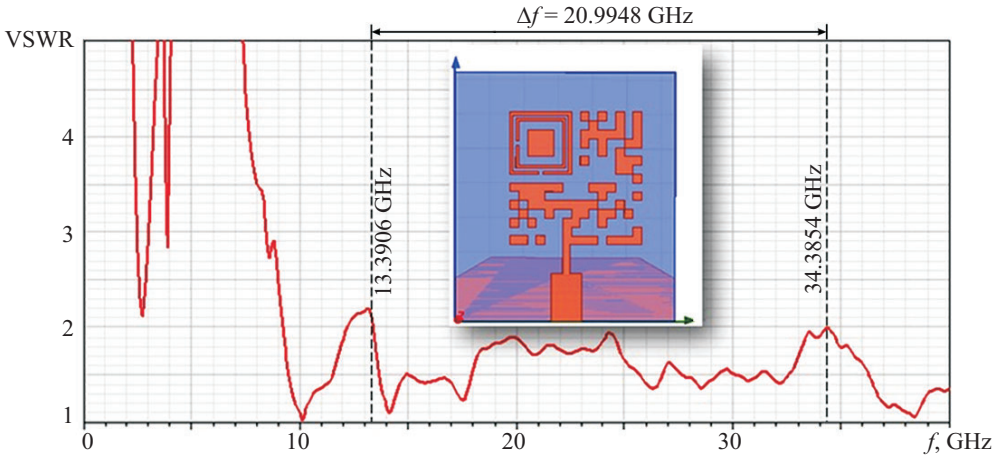

Fig. 13. Modification of antenna with angular separation of cutouts by 90° and its VSWR.

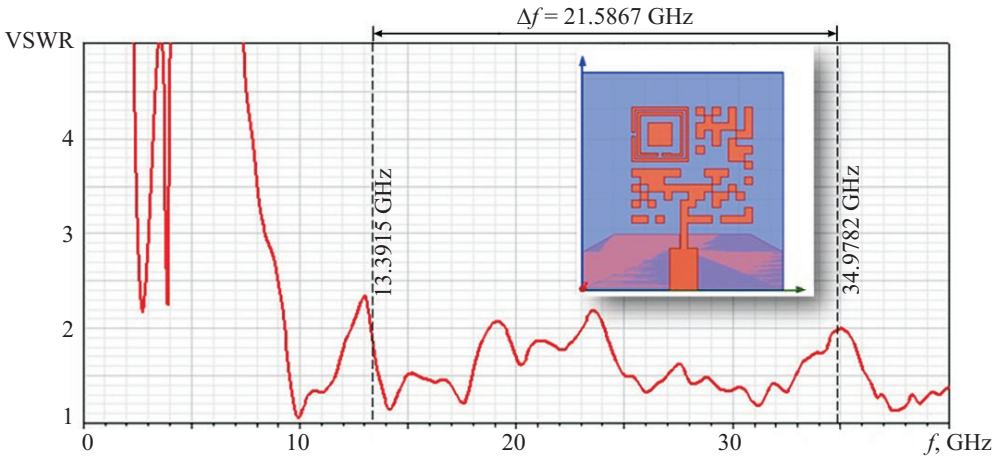

Fig. 14. Alternative design of antenna with angular separation of cutouts by 90° and its VSWR.

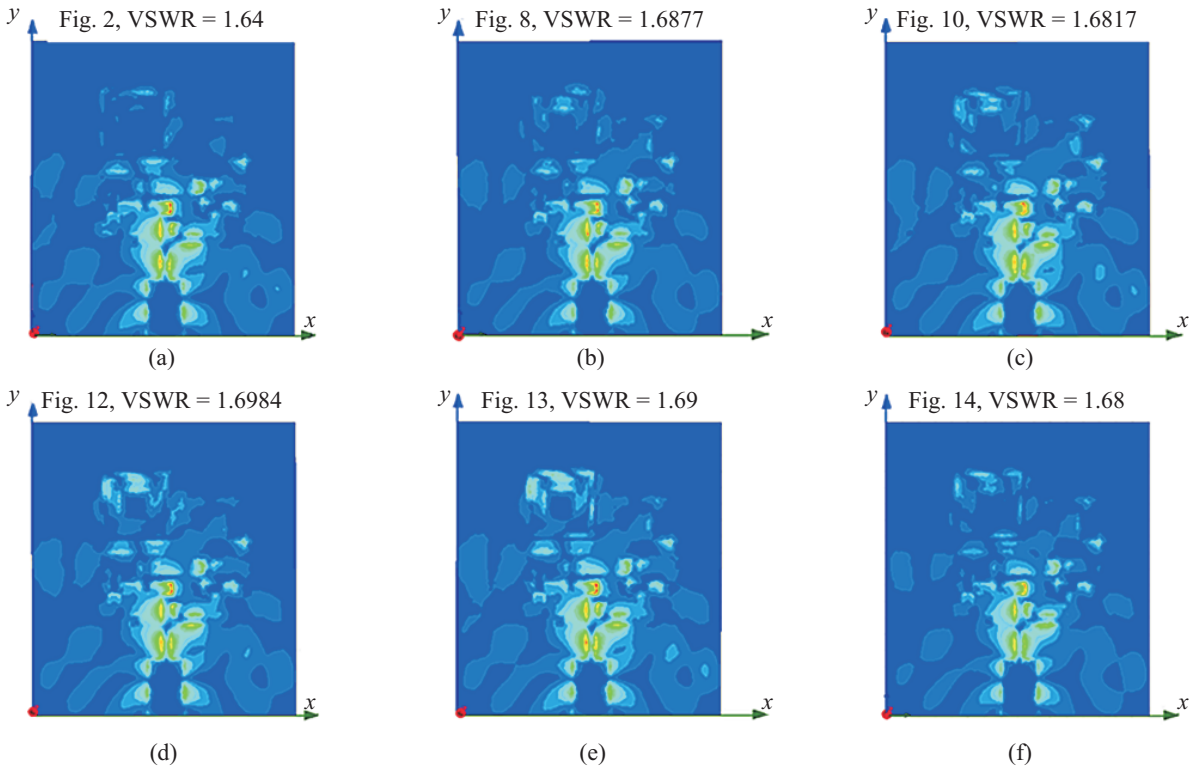

Fig. 15. Distribution of H-field at 25 GHz for entire scope of antenna topologies.

4. RESEARCH RESULTS FOR VARIOUS SRR ORIENTATIONS

Further investigation has been focused at the research on the influence of the cutouts' orientation in the SRR frame, integrated into the reference square pattern of the micro code, on the features of the patch antenna.

Figure 8 shows an orientation of the cutouts, which is an alternative to the above-described Fig. 2. In this case, the cutout of the outer "ring" is located above the reference point. As a result of the simulation, it turned out that the configuration in Fig. 8 is worse than that in Fig. 2.

The dependence of VSWR for an antenna in Fig. 8 is presented in Fig. 9. Along with the sharp rise of VSWR higher than level 2 in the frequency interval 34.43–35.1 GHz, insignificant exceedance of the threshold level of VSWR = 2.0303 can be seen at the frequency level of 22.468 GHz (Fig. 9).

The horizontal orientation of the cutouts in Fig. 10 option also separates the indicated frequency area of 167.935 GHz into several segments, limiting the first of its sectors by the interval from 13.52 to 33.1997 GHz (Fig. 11). Nevertheless, the presence of the continuous transmission bandwidth enables the estimation of the design in Fig. 10 to be more effective in comparison with Fig. 8.

The turn of the outer cutout of SRR to the right enabled us to obtain a slight shift of the upper level to 33.7576 GHz (Fig. 12) from 33.1997 GHz of the antenna in Fig. 10. Also, the bottom level of the corresponding range was slightly lowered (13.224 GHz). The total width of the working area of frequencies amounted to 20.53 GHz. In general, such a spectral segment covers the millimeter range of 5G waves [25]–[27], particularly NR operating bands n257 (26.5–29.5 GHz), n258 (24.25–27.5 GHz), n261 (27.5–28.35 GHz), and n260 (37–40 GHz), as well as the frequencies of the satellite communication Starlink of SpaceX company [28], [29].

Along with the classical design of square SRR, where the cutouts in frames are located along one axis [19]–[21], the modified options with the angular separation of the cutouts by 90° only, have been investigated as well. One such option is presented in Fig. 13. The cutout of the outer frame is located below, and the leftwards orientation of the cutout of the inner ring corresponds to the variable $Angle\_rotat\_In = 90°$.

It was found out that such a technical decision enables us to decrease the eruption at the frequency level of 34.3854 GHz to the level of VSWR = 1.9956, which formally implies that the bandwidth is still continuous at this frequency level as well.

The alternative option (Fig. 14) is characterized by the presence of spikes in VSWR values above 2.0 at 19 and 23.5 GHz.

The performed studies made it possible to establish the regularity in terms of the distribution of the electric and magnetic field components along the antenna surface, which characterizes the influence of the cutout orientation within the reference element on the quality of the antenna arrangement (VSWR level). The options of the H-field distribution at the frequency of 25 GHz for all reviewed antenna topologies are presented in Fig. 15, as the illustration of such dependency, including their corresponding VSWR values. As it follows from the presented distributions, the minimum VSWR value corresponds to the minimum radiance of the H-field in the region of reference SRR. The SRR presented in Fig. 2 possesses such minimum amplitude of H-field.

The present effect provides the engineers with an additional tool enabling them to improve the antenna arrangement based on the analysis of the distribution of H- and E-fields using optimization of the gap position in combination with the SRR lines width and the distance between them.

5. CONCLUSIONS

The key contribution of this study is the proposal of a novel approach for the design and synthesis of printed antennas using micro QR codes and metamaterial unit structures. The authors have shown that the use of SRR resonators as metamaterial unit structures can eliminate peaks in the frequency response, resulting in a continuous operating range with significantly higher bandwidth.

In particular, the formation of the metamaterial unit based on the reference element of the micro QR code enables us to expand the relative bandwidth of the corresponding printed antenna to a value of 1.7267 as compared to 0.8877 in paper [15]. This is important for the use of such antennas in 6G wireless systems.

The article describes studies conducted on the distribution of electric and magnetic field components along the surface of an antenna, which affects the quality of the antenna arrangement, as measured by a VSWR level. It was found that the distribution of the H-field at a frequency of 25 GHz varied across different antenna topologies, with the minimum VSWR value corresponding to the minimum radiance of the H-field in the region of a reference SRR. This finding provides engineers with an additional tool for improving antenna arrangement by optimizing the gap position, SRR line width, and distance between them based on the analysis of the distribution of H- and E-fields.

Since the estimation of the H-field brightness level is subjective, the optimal solution for optimizing the proposed antennas can involve the use of neural networks to determine the H-field brightness level in combination with a genetic algorithm for selecting metamaterial cell parameters.

The results of the study suggest that the proposed approach can be an effective solution for the design of patch antennas for use in radio frequency identification (RFID) tags and other wireless communication devices that require a small and efficient antenna for a wide range of applications. A similar approach has been summarized by the authors taking into consideration the cases of the synthesized antennas based on QR codes as well, however, the results of the corresponding studies deserve separate publications due to their significant volume.

The consequent efforts should be applied to the research of the influence of parameters of SRR-element on antenna characteristics. Moreover, attention should be paid to the investigation of other topologies of antennas of such types taking into consideration the coding of different phrases within micro QR code and different shapes of SRR elements. At that, the preferable ones are the codes possessing a symmetrical graphic structure toward the power supply leads.

The choice of the location of the switch point of the power supply leads has significant meaning as well, and during the scaling of the synthesized printed antennas concerning terahertz frequency range—the registration of the specific effects is important and attributable to nanoantennas [30]. Such specific effects in nanoantennas of terahertz frequency range include quantum confinements, localized surface plasmon resonance, nonlinear effects, etc.

The proposed concept of multi-layer integration of multiple micro QR patch antennas combines technological innovation and artistic design, providing the ability to create a platform that uses a fractal approach to form a hierarchical structure of QR codes. This fractal system, characterized by the use of the Kronecker product, the penetrating face product or block Kronecker product of matrices, allows for multi-level embedding of some QR codes into other QR codes, exponentially increasing the density of information and interaction possibilities within a single visual space.

ADDITIONAL INFORMATION

The initial version of this paper in Ukrainian is published in the journal *Izvestiya Vysshikh Uchebnykh Zavedenii. Radioelektronika*, ISSN 2307-6011 (Online), ISSN 0021-3470 (Print) on the link http://radio.kpi.ua/article/view/S002134702307004X with https://doi.org/10.20535/S002134702307004X.

FUNDING

This work was supported by ongoing institutional funding. No additional grants to carry out or direct this particular research were obtained.

CONFLICT OF INTEREST

The authors declare that they have no conflicts of interest.

REFERENCES

1. Z. E. Ankarali, B. Pekoz, H. Arslan, "Flexible radio access beyond 5G: A future projection on waveform, numerology, and frame design principles," *IEEE Access* **5**, 18295 (2017). https://doi.org/10.1109/ACCESS.2017.2684783.
2. T. S. Rappaport et al., "Wireless communications and applications above 100 GHz: Opportunities and challenges for 6G and beyond," *IEEE Access* **7**, 78729 (2019). https://doi.org/10.1109/ACCESS.2019.2921522.
3. M. H. Alsharif, M. A. M. Albreem, A. A. A. Solyman, S. Kim, "Toward 6G communication networks: Terahertz frequency challenges and open research issues," *Comput. Mater. Contin.* **66**, No. 3, 2831 (2021). https://doi.org/10.32604/cmc.2021.013176.
4. H. Zhang, B. Di, L. Song, Z. Han, *Reconfigurable Intelligent Surface-Empowered 6G* (Cham, Springer International Publishing, 2021). https://doi.org/10.1007/978-3-030-73499-2.
5. S. Zhao, B. Xie, Z. Liu, J. An, "Reconfigurable intelligent surface-assisted radar deception electronic counter-countermeasures," *Remote Sens.* **15**, No. 21, 5149 (2023). https://doi.org/10.3390/rs15215149.
6. V. I. Slyusar, "A family of face products of matrices and its properties," *Cybern. Syst. Anal.* **35**, No. 3, 379 (1999). https://doi.org/10.1007/BF02733426.
7. V. I. Slyusar, "Generalized face-splitting matrix products in models of digital antenna arrays with nonidentical channels," *Izvestiya Vysshikh Uchebnykh Zavedenij. Radioelektronika* **46**, No. 10, 15 (2003).
8. V. I. Slyusar, "New operations of matrix products for application of radars," in *IEEE MTT/ED/AP West Ukraine Chapter DIPED-97. Direct and Inverse Problems of Electromagnetic and Acoustic Theory* (*IEEE Cat. No.97TH8343*) (1997), pp. 73–74. https://doi.org/10.1109/DIPED.1997.710918.
9. D. Anagnostou, W. Cross, J. Meruga, J. Kellar, "Optically scannable code antenna," US Patent Application Publication US 2014/0263662 A1 (2014).
10. A. M. Numan-Al-Mobin, J. M. Meruga, W. M. Cross, J. J. Kellar, D. E. Anagnostou, "QR code antenna for wireless and security applications," in *2013 IEEE Antennas and Propagation Society International Symposium* (*APSURSI*) (2013), pp. 1728–1729. https://doi.org/10.1109/APS.2013.6711523.
11. A. M. Numan-Al-Mobin, J. M. Meruga, W. M. Cross, J. J. Kellar, D. E. Anagnostou, "QR code antennas for WiFi/WLAN/Bluetooth applications," in *IEEE International Conference on Electro-Information Technology*, *EIT 2013* (2013), pp. 1–2. https://doi.org/10.1109/EIT.2013.6632693.
12. A. Md Numan-Al-Mobin, W. M. Cross, J. J. Kellar, D. E. Anagnostou, "RFID integrated QR code tag antenna," in *2015 IEEE MTT-S International Microwave Symposium* (2015), pp. 1–3. https://doi.org/10.1109/MWSYM.2015.7167044.
13. G. S. Vardhan, N. Sivadasan, A. Dutta, "QR-code based chipless RFID system for unique identification," in *2016 IEEE International Conference on RFID Technology and Applications* (*RFID-TA*) (2016), pp. 35–39. https://doi.org/10.1109/RFID-TA.2016.7750744.
14. J. Doroshewitz, A. Kaur, J. Nanzer, P. Chahal, "Multi-factor product authentication using integrated Quick Response (QR) code pixelated antenna," *Int. Symp. Microelectron.* **2017**, No. 1, 000608 (2017). https://doi.org/10.4071/isom-2017-THA45_101.

15. V. Slyusar, I. Sliusar, "Micro QR code as the basis of patch antenna topologies," in *2021 IEEE International Conference on Information and Telecommunication Technologies and Radio Electronics* (*UkrMiCo*) (2021), pp. 31–34.
https://doi.org/10.1109/UkrMiCo52950.2021.9716614.
16. S. Bankov, A. Kurushin, *Calculation of Antennas and Microwave Structures Using HFSS Ansoft* [in Russian] (Moscow: Rodnik, 2009).
17. Online barcode generator.
https://barcode.tec-it.com/ru/MicroQR?data=antenna.
18. 3D Code Generator.
https://printer.tools/qrcode2stl.
19. V. Slyusar, "Metamaterials on antenna solutions," in *2009 IEEE 7th Int. Conf. on Antenna Theory and Techniques* (*ICATT'09*) (2009), pp. 19–24.
https://doi.org/10.1109/ICATT.2009.4435103.
20. V. Slyusar, "Metamaterials in the antenna equipment: basic principles and results," *First Mile* **3**, No. 4, 44 (2010).
21. I. Sliusar, V. Slyusar, Y. Utkin, O. Kopishynska, "Parametric synthesis of 3D structure of SRR element of the metamaterial," in *2020 IEEE International Conference on Problems of Infocommunications. Science and Technology* (*PIC S&T*) (2020), pp. 577–582.
https://doi.org/10.1109/PICST51311.2020.9468067.
22. I. Sliusar, L. Degtyareva, V. Slyusar, S. Voloshko, A. Zinchenko, "Synthesis of quasi-fractal ring antennas," in *2019 IEEE International Scientific-Practical Conference Problems of Infocommunications*, *Science and Technology* (*PIC S&T*) (2019), pp. 741–744.
https://doi.org/10.1109/PICST47496.2019.9061286.
23. I. Sliusar, S. Voloshko, V. Slyusar, V. Smolyar, "Synthesis of quasi-fractal hemispherical dielectric resonator antennas," in *2018 International Scientific-Practical Conference Problems of Infocommunications. Science and Technology* (*PIC S&T*) (2018), pp. 313–316.
https://doi.org/10.1109/INFOCOMMST.2018.8632087.
24. B. T. T. Center, "Assessment of ultra-wideband (UWB) technology," Contract No. DAAH01-88-C-0131, ARPA Order 6049 (1990).
https://apps.dtic.mil/sti/tr/pdf/ADA233624.pdf.
25. 5G NR (Rel-15).
https://www.3gpp.org/lte-2.
26. 5G NR (Rel-17).
https://www.3gpp.org/lte-2.
27. Prachi Gupta, "Performance improvement of millimeter wave antennas (review)", *Radioelectron. Commun. Syst.* **65**, No. 9, 527 (2022).
https://doi.org/10.20535/S0021347022100016.
28. A. Aguilar et al., "Tradespace exploration of the next generation communication satellites," in *AIAA Scitech 2019 Forum* (2019).
https://doi.org/10.2514/6.2019-0768.
29. USA SpaceX, "Starlink Kit 01437829-004, Regulatory Notices" (2021).
30. V. Slyusar, "Nanoantennas. Approaches and prospects," *Electron. Sci. Technol. Bus.*, No. 2, 58 (2009).
https://www.electronics.ru/journal/article/178.